probe outside the micellar surface, where the hydrophobic tail groups of the surfactant molecules were suggested to have a radial distribution to achieve a small density of the methyl groups near the center of the micelles (Figure 13a of ref 6).

The possibility of a nonspherical shape[34] of the micelles has also been investigated in the present case. The incorporation of iron porphyrin might lead to a prolate ellipsoidal shape of the micelles with short semiaxis[25] of 17.4 Å (radius of the spherical micelle) and long semiaxis of 30.8 Å. Figure 10 shows the variation in the average value of the short semiaxes (R_A) of the ellipsoids containing the micellar atoms. The average value of ($1/R_{IS}^6$) for the ellipsoid was evaluated by numerical integration of eq 11 over the ellipsoid using Gaussian quadrature formula.[35] Two different situations were considered: (i) both the micellar carbon and the iron center form ellipsoids inside the micelles with short semiaxes R_A and R_M, respectively (Figure 10a) and (ii) the iron center makes a sphere while the micellar carbons form ellipsoid around it (Figure 10b). The values of R_M for the case (i) were found to be 9.2 and 9.3 Å for aquahydroxo- and bis(cyano)hemin, respectively, while in the second case (ii), R_M was 15.3 Å for aquahydroxo- and 14.7 Å for the bis(cyano) complex.

Figure 10 shows that the overall nature of the distribution of micellar carbons inside the micelles is very similar to that observed with a spherical model of the micelles (Figure 9). The iron center of the porphyrin in all these models is quite embedded inside the micellar core. Moreover, similar results were obtained with a spherical micellar shape[36,37] of radius 15.8 Å. This indicates that the relative distribution of the micellar atoms inside the micelles containing the heme does not depend on the actual size or shape of the micelles, and in all these models the heme iron resides at the side of the micellar core. The position of the heme complex inside the micelles was found to depend on the type of the model considered. The iron atom in the porphyrin ring resides ~5 Å inside the micellar radius for the spherical model, while this distance is not constant for the ellipsoidal models. However, in all the models considered, the iron porphyrin moiety is definitely embedded inside the hydrophobic micellar core. The total error in determination of the radial distances of different carbons from the center of the micelle was ≤10%, estimated from the experimental errors and the subsequent approximations in correlation times made in the calculations.

(34) Ben-Naim, A.; Stillinger, F. H. *J. Phys. Chem.* **1980**, *84*, 2872.
(35) Marathe, V. R.; Mitra, S. *Chem. Phys. Lett.* **1974**, *27*, 103.
(36) Reiss Husson, F.; Luzzati, V. *J. Colloid Interface Sci.* **1966**, *21*, 534.
(37) Reiss Husson, F.; Luzzati, V. *J. Phys. Chem.* **1964**, *68*, 3504.

Conclusions

The structural disposition of the ferric porphyrins inside aqueous detergent micelles determined in this paper suggests that these complexes are embedded inside the micellar Stern layer, with the hydrophilic propionate side chains of the porphyrin ring directed toward the polar surface of the micelles. We have assumed a smooth surface of the micelles and a uniform probability distribution of the detergent and heme centers so that the average value of ($1/R_{IS}$) could be evaluated by simple integration over the micelle. A spherical micelle with larger aggregation number ($\bar{N}$) has been suggested to be a very suitable model for this system. Since the critical micellar concentration of the micelles does not show any drastic change on addition of the ferric heme complex, the assumption of spherical micelles seems to be valid under the experimental conditions. The structural parameters were deduced in the present study from the average distances between the surfactant carbons and the heme iron center, which gave only a statistically averaged picture of the micelles rather than the exact structure of the aggregate. A detailed analysis of the experimental results for different ellipsoidal structures showed that although the absolute values of the distance parameters depend on the radius and shape of the micelles the relative distribution of the micellar atoms inside the micellar core is more or less independent of the type of model. Thus, the assumption made in using an average value of aggregation number does not affect the overall picture of the heme inside micelles. Since the distance parameters were evaluated from T_{1M} by using the Solomon-Bloembergen equation (eqs 9 and 10), the small errors because of the neglect of K_D and simplification of τ_C in the evaluation of T_{1M} do not essentially affect the final results.

Acknowledgment. The NMR work reported here was done at the 500-MHz FT NMR National Facility. The author thanks Mr. V. Subrahmanyam, D. G. Maharana, and Dr. O. K. Medhi for help and Prof. Samaresh Mitra for encouragement and advice.

Light Scattering of Spinnable, Viscoelastic Solutions of Hexadecyltrimethylammonium Salicylate

Toyoko Imae

Department of Chemistry, Faculty of Science, Nagoya University, Chikusa, Nagoya 464, Japan
(Received: October 17, 1989; In Final Form: February 19, 1990)

Static, dynamic, and electrophoretic light scattering were measured for spinnable, viscoelastic solutions of hexadecyltrimethylammonium salicylate with and without sodium salicylate (NaSal) at various temperatures. While short rodlike micelles are formed in aqueous solutions without NaSal, the length of rodlike micelles increases with an increase in NaSal concentration and reaches 2000–3000 nm in 0.1 M NaSal. However, the size diminishes above 0.5 M NaSal, and small micelles exist in 1 M NaSal. The external interference effect indicating a strong intermicellar correlation is quite apparent in aqueous solutions without NaSal, but it decreases with addition of NaSal and is imperceptible above 0.001 M NaSal. The electrophoretic mobility changes sign from positive to negative with addition of 0.1 M NaSal, indicating the reversal of the net micelle charge. The pseudolinkages between short rodlike micelles, in which salicylate ions participate, would be constructed in aqueous solutions without or with a small amount of NaSal, and the entanglement of long rodlike micelles exists, besides the pseudolinkages, in aqueous solutions with a medium amount of NaSal.

Introduction

The thread-forming property of a liquid, i.e., its "spinnability", is a phenomenon that is frequently observable for native and synthetic polymers. Similar characteristics have been observed for aqueous solutions of cationic surfactants with certain kinds of aromatic counterions, and many investigations have been reported, mainly regarding solution viscoelasticity.[1-17] Nevertheless,

(1) Ulmius, J.; Wennerström, H.; Johansson, L. B.-Å.; Lindblom, G.; Gravsholt, S. *J. Phys. Chem.* **1979**, *83*, 2232.

0022-3654/90/2094-5953$02.50/0

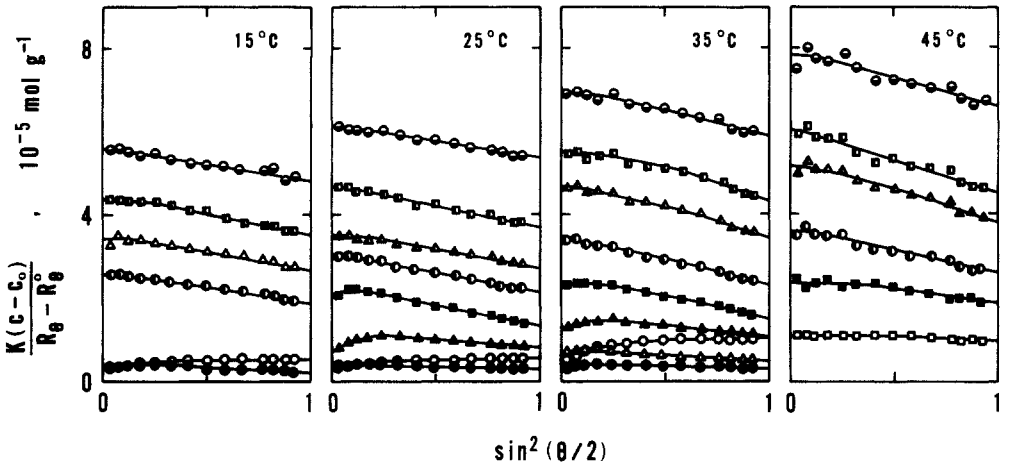

Figure 1. Angular dependence of static light scattering for aqueous solutions of C_{16}TASal without NaSal at various temperatures. Micelle concentration (10^{-2} g cm^{-3}): ○, 0.017; △, 0.034; □, 0.049; ●, 0.066; ▲, 0.094; ■, 0.200; ◐, 0.302; ◭, 0.448; ◧, 0.600; ◒, 0.987.

TABLE I: Specific Refractive Index Increment for Aqueous NaSal Solutions of C_{16}TASal (in Units of cm^3 g^{-1})

	T, °C			
C_s, M	15	25	35	45
0	0.179	0.177	0.175	0.176
0.1	0.174	0.166	0.154	0.150
1.0	0.141	0.147	0.150	0.149

the mechanism for the spinnability and viscoelasticity of aqueous surfactant solutions has not been clearly identified.

Recently, we[18] have quantitatively measured the spinnability of aqueous salt solutions of tetradecyl- and hexadecyltrimethylammonium salicylates (C_{14}TASal and C_{16}TASal). There were two types of spinnability, which exhibited three extremes when plotted against NaSal concentration.

In this paper, we present light scattering studies from spinnable, viscoelastic solutions of C_{16}TASal, and the size and structure of micelles in aqueous solutions with and without NaSal are discussed in connection with a proposed mechanism for the spinnable behavior.

Experimental Section

The sample of C_{16}TASal is the same as previously prepared and used.[18] Commercial NaSal was used without any purification. Water was prepared by a routine method.

Light scattering intensity, mutual diffusion coefficient, specific refractive index increment, and electrophoretic drift velocity were measured on dynamic light scattering spectrophotometer DLS-700, differential refractometer RM-102, and electrophoretic light scattering spectrophotometer ELS-800, all of which were manufactured by Otsuka Electronics, Co. Ltd., Osaka. The details of the experimental procedure are described elsewhere.[19-22] Numerical values of the specific refractive index increment are given in Table I for various NaSal concentrations C_s and temperatures.

Results

Light Scattering for Aqueous Solutions without NaSal. The light scattering was measured for aqueous solutions of C_{16}TASal without NaSal at 15–45 °C. The critical micelle concentration c_o, above which the reduced scattering intensity increases, was determined as 0.006×10^{-2} g cm^{-3} (1.5×10^{-4} M), which is consistent with that previously reported.[5]

Figure 1 represents the angular dependence of static light scattering for aqueous solutions of C_{16}TASal without NaSal. The reciprocal angular envelope of light scattering increases with the scattering angle, θ, for dilute solutions of $(0.017–0.025) \times 10^{-2}$ g cm^{-3}, according to the relation of

$$K(c - c_o)/(R_\theta - R_\theta^\circ) = 1/MP(\theta) + 2B_2(c - c_o) \quad (1)$$

with

$$1/P(\theta) = 1 + (1/3)R_G^2\mu^2 \quad (2)$$

where K is the optical constant. R and R° represent the reduced scattering intensities at the surfactant concentration, c, and the critical micelle concentration, c_o, respectively. M is the molecular weight, R_G is the radius of gyration, B_2 is the second virial coefficient, $P(\theta)$ is the particle scattering factor originating in the internal interference effect, and μ is the magnitude of scattering vector.

On the basis of the equation

$$\lim_{\theta \to 0} K(c - c_o)/(R_\theta - R_\theta^\circ) \equiv K(c - c_o)/(R_\theta - R_\theta^\circ)$$
$$= 1/M + 2B_2(c - c_o) + 3B_3(c - c_o)^2$$
$$\equiv 1/M_{app} \quad (3)$$

where B_3 is the third virial coefficient, the apparent molecular weight, M_{app}, at 0.017×10^{-2} g cm^{-3} (5×10^{-4} M) was evaluated as 3.2×10^4, 3.7×10^4, and 1.8×10^4 at 15, 25, and 35 °C, respectively. These molecular weights correspond to aggregation numbers of 740, 880, and 440, respectively, indicating that short rodlike micelles are formed in aqueous solutions of C_{16}TASal without NaSal.

(2) Hoffmann, H.; Platz, G.; Rehage, H.; Schorr, W. *Ber. Bunsen-Ges. Phys. Chem.* **1981**, *85*, 877.
(3) Hoffmann, H.; Platz, G.; Rehage, H.; Schorr, W. *Adv. Colloid Interface Sci.* **1982**, *17*, 275.
(4) Rehage, H.; Hoffmann, H. *Faraday Discuss. Chem. Soc.* **1983**, *76*, 363.
(5) Angel, M.; Hoffmann, H.; Löbl, M.; Reizlein, K.; Thurn, H.; Wunderlich, I. *Prog. Colloid Polym. Sci.* **1984**, *69*, 12.
(6) Thurn, H.; Löbl, M.; Hoffmann, H. *J. Phys. Chem.* **1985**, *89*, 517.
(7) Hoffmann, H.; Löbl, H.; Rehage, H.; Wunderlich, I. *Tenside Deterg.* **1985**, *22*, 290.
(8) Olsson, U.; Söderman, O.; Guêring, P. *J. Phys. Chem.* **1986**, *90*, 5223.
(9) Rehage, H.; Wunderlich, I.; Hoffmann, H. *Prog. Colloid Polym. Sci.* **1986**, *72*, 51.
(10) Rao, U. R. K.; Manohar, C.; Valaulikar, B. S.; Lyer, R. M. *J. Phys. Chem.* **1987**, *91*, 3286.
(11) Kalus, J.; Hoffmann, H. *J. Chem. Phys.* **1987**, *87*, 714.
(12) Shikata, T.; Sakaiguchi, Y.; Uragami, H.; Tamura, A.; Hirata, H. *J. Colloid Interface Sci.* **1987**, *119*, 291.
(13) Shikata, T.; Hirata, H., Kotaka, T. *Langmuir* **1987**, *3*, 1081.
(14) Rehage, H.; Hoffmann, H. *J. Phys. Chem.* **1988**, *92*, 4712.
(15) Shikata, T.; Hirata, H.; Kotaka, T. *Langmuir* **1988**, *4*, 354.
(16) Shikata, T.; Hirata, H.; Takatori, E.; Osaki, K. *J. Non-Newtonian Fluid Mech.* **1988**, *28*, 171.
(17) Bewersdorff, H.-W.; Ohlendorf, D. *Colloid Polym. Sci.* **1988**, *266*, 941.
(18) Imae, T.; Hashimoto, K.; Ikeda, S. *Colloid Polym. Sci.*, in press.
(19) Imae, T.; Ikeda, S. *Colloid Polym. Sci.* **1987**, *265*, 1090.
(20) Imae, T. *J. Phys. Chem.* **1988**, *92*, 5721.
(21) Imae, T. *J. Colloid Interface Sci.* **1989**, *127*, 256.
(22) Imae, T.; Otani, W.; Oka, K. *J. Phys. Chem.* **1990**, *94*, 853.

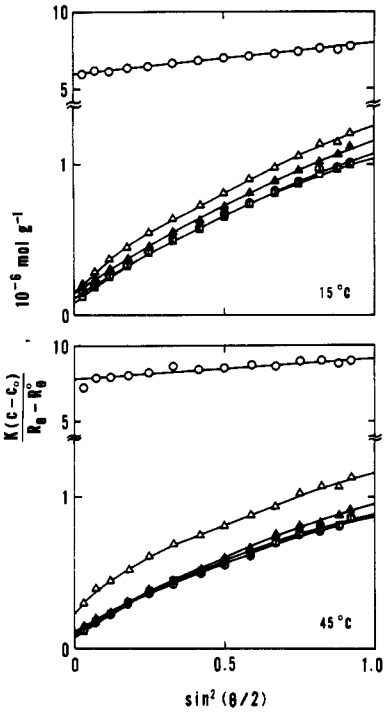

Figure 2. Angular dependence of static light scattering for 0.1 M NaSal solutions of C_{16}TASal at 15 and 45 °C. Micelle concentration (10^{-2} g cm^{-3}): ○, 0.039; △, 0.070; □, 0.099; ⊕, 0.153; ▲, 0.200.

On the other hand, for aqueous solutions above 0.034×10^{-2} g cm^{-3}, the reciprocal angular envelope of light scattering decreases with an increase in sin^2 (θ/2), some curves exhibiting a maximum. Such unusual behavior is contributed to by the strong effect of external interference. Then the reduced scattering intensity of light scattering must be described by

$$R_\theta - R_\theta^\circ = K(c - c_o)MP(\theta)S(\theta) \quad (4)$$

where $S(\theta)$ is the structure factor arising from the external interference effect.[23-27] The external interference effect, i.e., the intermicellar correlation, strengthens with increasing micelle concentration, $c - c_o$, and with rising temperature. Similar unusual behavior in the angular dependence of light scattering intensity was previously reported for aqueous solutions of oleyldimethylamine oxide.[28,29]

The mutual diffusion coefficient, D, is described by

$$D = D_d(\theta)D_i(c-c_o,\theta)$$

$$= D_d(\theta)[1 - (\bar{v} + k_f)(c - c_o)]MK(c - c_o)/(R_\theta - R_\theta^\circ) \quad (5)$$

where D_d and D_i are the terms associated with the diffusion coefficients and the internal and external interference effects, respectively. $\bar{v}$ is the partial specific volume and k_f is the frictional virial coefficient. Therefore, the strong external interference effect may also affect the mutual diffusion coefficient. Actually, the mutual diffusion coefficient for aqueous solutions of C_{16}TASal without NaSal depended on sin^2 (θ/2) and increased with an increase in micelle concentration.

Light Scattering for 0.1 M NaSal Solutions. For 0.1 M NaSal solutions of C_{16}TASal, the critical micelle concentration estimated from the reduced scattering intensity is lower than 10^{-5} g cm^{-3}. The angular dependence of static light scattering at 15 and 45 °C is drawn in Figure 2. A similar angular dependence was observed at 25 and 35 °C. The reciprocal angular envelope of static light scattering barely depends on temperature.

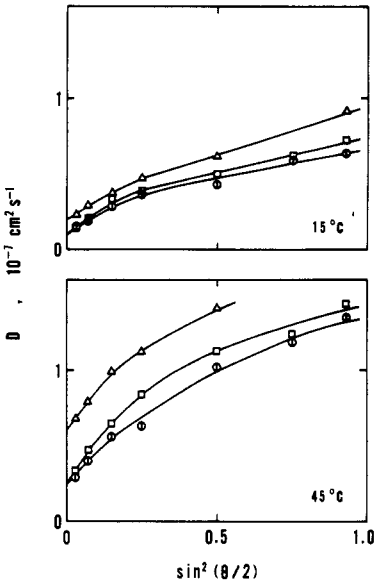

Figure 3. Angular dependence of dynamic light scattering for 0.1 M NaSal solutions of C_{16}TASal at 15 and 45 °C. The symbols represent the same micelle concentrations as in Figure 2.

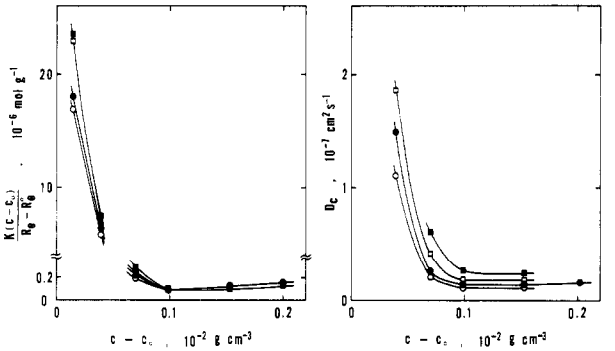

Figure 4. $K(c - c_o)/(R_\theta - R_\theta^\circ)$ and D_c values plotted against micelle concentration for 0.1 M NaSal solutions of C_{16}TASal. Temperature (°C): ○, 15; ●, 25; □, 35; ■, 45.

Different from aqueous solutions of C_{16}TASal without NaSal, the reciprocal angular envelope of static light scattering for 0.1 M NaSal solutions always increases with sin^2 (θ/2) at micelle concentrations of (0.014–0.20) $\times 10^{-2}$ g cm^{-3} examined here. Moreover, the reciprocal angular envelope has an upward convex curvature at high micelle concentrations above 0.070×10^{-2} g cm^{-3}, indicating the formation of rodlike micelles.[29,30]

The upward convex curvature of mutual diffusion coefficient against sin^2 (θ/2) was observed simultaneously, as shown in Figure 3. This is characteristic of rodlike micelles in dilute and semidilute solutions and suggests that there is a contribution of rotational diffusion, besides translational diffusion, on the mutual diffusion coefficient.[31] The angular dependence of the mutual diffusion coefficient increases slightly with temperature.

Same concluding remarks can be obtained from Figure 4, where the reciprocal scattering intensity, $K(c - c_o)/(R_\theta - R_\theta^\circ)$, and the mutual diffusion coefficient, D_c, extrapolated to zero scattering angle are plotted. Then

$$\lim_{\theta \to 0} D \equiv D_c = D_o[1 + k_D(c - c_o)] \quad (6)$$

with

$$k_D = 2B_2M - k_f - \bar{v} \quad (7)$$

(23) Ehrlich, G.; Doty, P. *J. Am. Chem. Soc.* **1954**, *76*, 3764.
(24) Burchard, W. *Polymer* **1969**, *10*, 29.
(25) Brown, J. D.; Pusey, P. N.; Goodwin, J. W.; Ottewill, R. H. *J. Phys. A: Math. Gen.* **1975**, *8*, 664.
(26) Shaefer, D. *J. Chem. Phys.* **1977**, *66*, 3980.
(27) Nieuwenhuis, E. A.; Vrij, A. *J. Colloid Interface Sci.* **1979**, *72*, 321.
(28) Imae, T.; Ikeda, S. *J. Colloid Interface Sci.* **1984**, *98*, 363.
(29) Imae, T.; Ikeda, S. *Colloid Polym. Sci.* **1985**, *263*, 756.
(30) Imae, T.; Ikeda, S. *Colloid Polym. Sci.* **1984**, *262*, 497.
(31) Imae, T. *J. Phys. Chem.* **1989**, *93*, 6720.

TABLE II: Characteristics of Spherical Micelles of $C_{16}TASal$ in 1 M NaSal Solutions at Various Temperatures

T, °C	$10^2(c - c_0)$, g cm^{-3}	$10^{-4}M$	m	10^7D_0, cm^2 s^{-1}	R_H, nm	b, nm	10^4B_2, mol cm^3 g^{-2}	10^3B_3, mol cm^6 g^{-3}	k_f, cm^3 g^{-1}	K_D, cm^3 g^{-1}
15	0[a]	4.98	118	5.25	2.42					
	0.40	4.89	116	4.54	2.89	4.99	1.02	0.32	8.2	0.56
	0.70	5.54	131	4.11	3.19	6.71	1.08	0.40	9.8	0.67
	1.01	6.31	150	3.83	3.43	8.34	1.02	0.41	10.6	0.73
25	0[a]	3.70	88	7.50	2.21					
	0.19	4.08	97	7.40	2.24	2.32	0.68	0.12	4.6	0.31
	0.40	3.93	86	6.50	2.55	3.43	1.09	0.29	7.0	0.48
	0.70	4.79	114	5.80	2.86	4.83	1.03	0.32	8.1	0.55
	1.01	6.22	148	4.18	3.97	12.9	1.63	1.04	16.6	1.14
35	0[a]	2.80	66	9.90	2.15					
	0.40	3.47	104	7.66	2.68	3.98	1.62	0.57	9.2	0.63
	0.70	4.93	117	5.95	3.45	8.48	1.71	0.90	13.8	0.95
	1.01	5.96	141	5.47	3.75	11.0	1.50	0.84	14.7	1.01
45	0[a]	2.56	61	11.5	2.15					
	0.19	2.84	67	11.7	2.12		1.21	0.26	5.6	0.39
	0.40	3.33	79	9.92	2.50	3.23	1.42	0.42	7.8	0.53
	0.70	4.14	98	7.29	3.40	8.12	2.32	1.39	15.7	1.08
	1.01	4.85	115	7.02	3.53	9.09	1.89	1.08	15.0	1.03

[a] Calculated from the $K(c - c_0)/(R_\theta - R_\theta°)$ and D_c values extrapolated to zero micelle concentration.

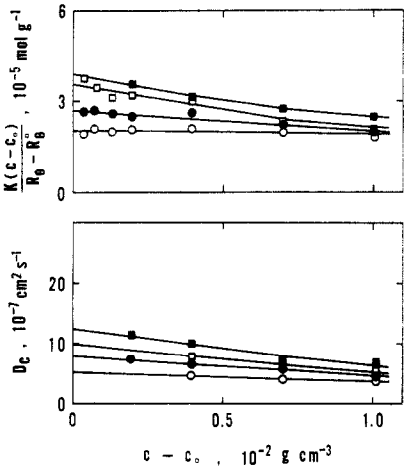

Figure 5. $K(c - c_0)/(R_\theta - R_\theta°)$ and D_c values plotted against micelle concentration for 1 M NaSal solutions of $C_{16}TASal$. The symbols represent the same temperatures as in Figure 4.

where D_0 is the total translational diffusion coefficient and k_D is the hydrodynamic virial coefficient. It is noticed that an apparent micellar size increases remarkably at micelle concentrations up to 0.1×10^{-2} g cm^{-3}, while it changes scarcely at $(0.1–0.2) \times 10^{-2}$ g cm^{-3}.

Light Scattering for 1 M NaSal Solutions. Despite that the critical micelle concentration of $C_{16}TASal$ in 1 M NaSal is less than 10^{-5} g cm^{-3} as well as that in 0.1 M NaSal, the reciprocal scattering intensity and the mutual diffusion coefficient for 1 M NaSal solutions of $C_{16}TASal$ are larger than those for 0.1 M NaSal solutions. Moreover, they are independent of scattering angle.

The reciprocal scattering intensity and the mutual diffusion coefficient at zero scattering angle, which are represented in Figure 5, decrease with increasing micelle concentration. The decrease is more gradual at lower temperature and more rapid at higher temperature.

Molecular weight and hydrodynamic radius, R_H, of micelles can be calculated by

$$\lim_{\substack{\theta\to 0\\ c\to 0}} K(c - c_0)/(R_\theta - R_\theta°) = 1/M \tag{8}$$

and

$$\lim_{\substack{\theta\to 0\\ c\to 0}} D = D_0 = k_B T/6\pi\eta_0 R_H \tag{9}$$

where k_B is the Boltzmann constant, T is the absolute temperature, and η_0 is the viscosity of solvent. From numerical values that are given in Table II, it can be interpreted that molecules of $C_{16}TASal$ in 1 M NaSal associate into small micelles. The aggregation number, m ($=M/421.6$), increases from 61 at 45 °C to 118 at 15 °C, and the hydrodynamic radius ranges from 2.2 to 2.4 nm, indicating the variation of micellar shape from sphere to ellipsoid.

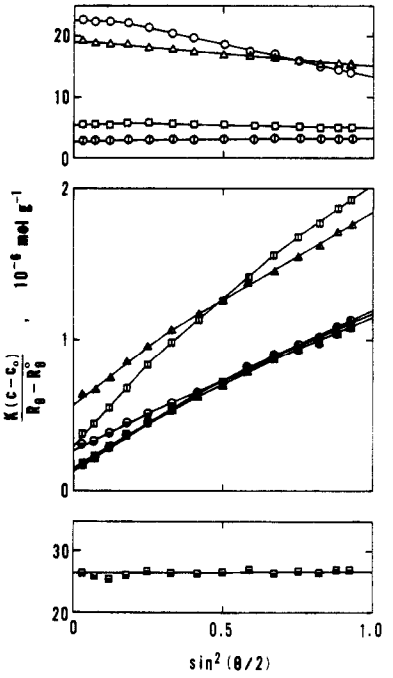

Figure 6. Angular dependence of static light scattering for aqueous NaSal solutions of $C_{16}TASal$ at 25 °C. $c = 0.2 \times 10^{-2}$ g cm^{-3}. NaSal concentration (M): ○, 0; △, 0.0001; □, 0.0005; ⊕, 0.001; ▲, 0.005; ⊞, 0.01; ◐, 0.05; ▲, 0.1; ⊡, 0.2; ◒, 0.5; ■, 1.0.

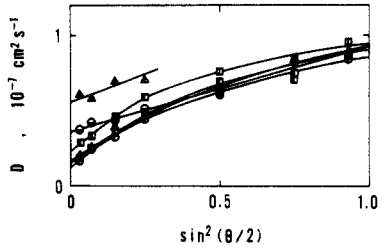

Figure 7. Angular dependence of dynamic light scattering for aqueous NaSal solutions of $C_{16}TASal$ at 25 °C. $c = 0.2 \times 10^{-2}$ g cm^{-3}. The symbols represent the same NaSal concentrations as in Figure 6.

Light Scattering for Aqueous Solutions with Various NaSal Concentrations. The light scattering for aqueous solutions of

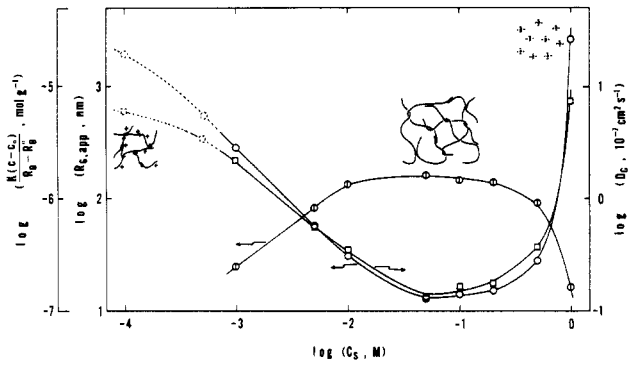

Figure 8. Double logarithmic plots of $K(c - c_o)/(R_\theta - R_\theta°)$, $R_{G,app}$, and D_c vs C_s for aqueous NaSal solutions of C_{16}TASal at 25 °C and schematic models of typical micelle structures. $c = 0.2 \times 10^{-2}$ g cm^{-3}. ○, $K(c - c_o)/(R_\theta - R_\theta°)$; ●, $R_{G,app}$; □, D_c. The contribution of external interference effect is included in the region of dotted lines.

TABLE III: Electrophoretic Light Scattering Data of C_{16}TASal Micelles at 25 °C ($c = 0.055 \times 10^{-2}$ g cm^{-3})

C_s, M	θ, deg	E, V cm^{-1}	$10^2 v$, cm s^{-1}	$10^4 U$, cm^2 V^{-1} s^{-1}
0	10	49.8	2.16	4.34
0.01	20	29.6	0.48	1.62
0.10	20	33.4	−0.063	−0.19

C_{16}TASal at 0.20×10^{-2} g cm^{-3} (0.005 M) with various NaSal concentrations was measured at 25 °C and plotted in Figures 6 and 7. It may be noted from Figure 6 that the contribution of external interference effect inducing the unusual angular dependence of static light scattering diminishes with an addition of NaSal and cannot be detected at NaSal concentrations above 0.001 M. While the usual angular dependence of static light scattering with an upward convex curvature is observed in the presence of 0.005–0.5 M NaSal, the static light scattering for 1 M NaSal solution is independent of scattering angle.

The mutual diffusion coefficient measured in an addition of 0.005–0.2 M NaSal increases with an upward convex curvature with an increase of $\sin^2(\theta/2)$, as seen in Figure 7, while for 0.5 M NaSal solutions it increases linearly with $\sin^2(\theta/2)$.

Double logarithmic plots of $K(c - c_o)/(R_\theta - R_\theta°)$ and D_c vs C_s are given in Figure 8, which includes values of apparent radius of gyration, $R_{G,app}$, evaluated from the equation

$$K(c - c_o)/(R_\theta - R_\theta°) = (1/M_{app})[1 + (1/3)R_{G,app}{}^2\mu^2] \quad (10)$$

Around 0.05 M NaSal, the $K(c - c_o)/(R_\theta - R_\theta°)$ and D_c values exhibit minima and the $R_{G,app}$ values present a maximum, suggesting the formation of longest rodlike micelles.

Electrophoretic Light Scattering. When the electric field, E, was applied, the electrophoretic drift velocity, v, which is evaluated from a Doppler shift value on the light scattering power spectrum, was measured for aqueous NaSal solutions of C_{16}TASal of 0.055 $\times 10^{-2}$ g cm^{-3} at 25 °C. Then the electrophoretic mobility, U, is calculated by

$$U = v/E \quad (11)$$

and listed in Table III with numerical values of related parameters. The mobility, which is 4.34×10^{-4} cm^2 V^{-1} s^{-1} for aqueous solution without NaSal, decreases with an addition of NaSal: it converts the sign to negative in the presence of 0.1 M NaSal.

It can be mentioned that C_{16}TASal micelles in water exhibit positive electrostatic potential. The electrostatic potential decreases with an addition of NaSal, owing to the strong adsorption of salicylate ions on a Stern layer surface of micelle. The excess adsorption of salicylate ions occurs above 0.1 M NaSal, inducing the negative electrostatic potential at a sliding plane, i.e., the negative ζ potential.

Discussion

When NaSal was added to aqueous solutions of C_{16}TASal, the size of micelles increased with an addition of NaSal up to 0.05 M, while it diminished at higher NaSal concentrations. This salt effect of NaSal was very different from that of NaCl and NaBr. The addition of the latter salts always promoted the formation of larger micelles.[19,20,29,30,32,33] The effect of added salt was remarkably different in the spinnability for aqueous salt solutions of C_{14}TASal.[18] The spinnability disappeared in the presence of 0.5 M NaSal, whereas aqueous NaBr solutions of C_{14}TASal were spinnable even in an addition of 2 M NaBr. The difference was observed even in the liquid–liquid phase separation phenomenon in aqueous solutions of heptaoxyethylene tetradecyl ether.[34] Although the addition of NaCl lowered the lower critical solution temperature (LCST), the LCST was raised in the presence of NaSal.

Different from bromide ions which bind electrostatically on a micelle surface, salicylate ions penetrate into a micelle.[8] While NaCl or NaBr always produces the salting-out effect, large amounts of NaSal affect C_{16}TASal micelles differently due to the specific binding behavior of salicylate ion. Then large amounts of salicylate counterion bind to a micelle, and the net surface charge varies sign, if the counterion binding is excess. Electrophoretic light scattering measurement confirmed that the ζ potential of C_{16}TASal micelle already changed its sign in an addition of 0.1 M NaSal.

Molecules of C_{16}TASal associate into rodlike micelles in aqueous solutions without NaSal. According to the procedure previously reported,[33] and utilizing the aggregation number, 61, and the radius, 2.2 nm, of spherical micelles, the length of rodlike micelles can be estimated as 29 and 34 nm in aqueous solutions of C_{16}TASal of 0.017×10^{-2} g cm^{-3} (5×10^{-4} M) at 15 and 25 °C, respectively. Rehage and Hoffmann[4] calculated the lengths of rodlike micelles of C_{16}TASal as 38.5 and 44.0 nm for surfactant solutions of 0.001 and 0.002 M, respectively, at 20 °C from viscosity data on the basis of the theory of Doi and Edwards for stiff rods. The lengths estimated here are not inconsistent with values by Rehage and Hoffmann.

For 0.1 M NaSal solutions of C_{16}TaSal where long rodlike micelles are formed, the analysis method[35] was applied for light scattering data at a finite micelle concentration and the numerical values of micellar size and micellar interaction were obtained for micellar solutions of 0.099×10^{-2} g cm^{-3}, as shown in Table IV.

It is noteworthy that the temperature dependence of numerical values is not remarkable. Aggregation number, radius of gyration, and hydrodynamic radius are comparable with or slightly larger than those for tetradecyldimethylammonium chloride (C_{14}DAC) in 2.6 M NaCl and tetradecyldimethylammonium bromide (C_{14}DAB) in 4.3 M NaBr.[35] Since a kind of flexibility parameter, $\rho \equiv R_G/R_H$, ranges from 1.6 to 1.8, rodlike micelles of C_{16}TASal can be regarded as semiflexible as well as rodlike micelles of C_{14}DAC, C_{14}DAB, and heptaoxyethylene alkyl ethers (C_nE_7).[20,35] The second virial coefficient and the frictional virial coefficient are larger than those for C_{14}DAC, C_{14}DAB, and C_nE_7,[20,35] suggesting that there is stronger interaction or correlation between C_{16}TASal micelles. The hydrodynamic virial coefficient is smaller than the frictional virial coefficient owing to the compensation between large $2B_2M$ and k_f values.

On the basis of the equation

$$R_G{}^2/a^2 = L_c/3a - 1 + (2a/L_c)[1 - (a/L_c)(1 - e^{-L_c/a})] \quad (12)$$

and with the use of the obtained values of molecular weight and radius of gyration, the persistence length, a, of semiflexible rodlike micelles in 0.1 M NaSal was evaluated. The contour length, L_c, is related to molecular weight by

$$L_c = M/M_L \quad (13)$$

where M_L is the molecular weight per unit contour length and was calculated according to the method described previously.[33] The threshold micelle concentration of overlap, that is, the

(32) Imae, T.; Ikeda, S. *J. Colloid Interface Sci.* **1985**, *108*, 215.
(33) Imae, T.; Ikeda, S. *J. Phys. Chem.* **1986**, *90*, 5216.
(34) Imae, T.; Sasaki, M.; Abe, A.; Ikeda, S. *Langmuir* **1988**, *4*, 414.
(35) Imae, T. *Langmuir* **1989**, *5*, 205.

TABLE IV: Characteristics of Rodlike Micelles of C_{16}TASal in 0.1 M NaSal Solutions at Various Temperatures ($c - c_o = 0.099 \times 10^{-2}$ g cm^{-3})

T, °C	$10^{-4}M$	m	R_G, nm	10^7D_o, cm^2 s^{-1}	R_H, nm	ρ	10^5B_2, mol cm^3 g^{-2}	k_f, cm^3 g^{-1}	k_D, cm^3 g^{-1}	L_c, nm	a, nm	$L_c/2a$	$10^2(c - c_o)_w$*, g cm^{-3}
15	2760	65 400	306	0.097	190	1.61	2.73	1630	−125	2360	142	8.3	0.067
25	2640	62 500	294	0.142	165	1.78	2.68	1430	−14	2260	137	8.2	0.072
35	3310	78 500	310	0.158	184	1.68	3.28	2030	144	2830	115	12.3	0.084
45	3030	71 900	291	0.208	168	1.73	3.37	1890	153	2590	111	11.7	0.093

crossover concentration between dilute and semidilute regimes, $(c - c_o)_w$*, was, in turn, evaluated from the relation

$$(c - c_o)_w^* = 2^{3/2}M/[(aL_c)^{3/2}N_A] \quad (14)$$

for wormlike chains.[36] The numerical values are listed in Table IV with values of $L_c/2a$.

Although the contour length ranges from 2000 to 3000 nm and is in agreement with those for C_{14}DAC in 2.6 M NaCl and C_{14}DAB in 4.3 M NaBr,[37] the persistence length of 100–150 nm is 2 times longer than those of C_{14}DAC and C_{14}DAB micelles[37] and is close to that of oleyldimethylamine oxide micelle,[29] indicating the more rigid semiflexible character of C_{16}TASal micelles. The calculated $(c - c_o)_w$* values agree with the observed one. Since the threshold micelle concentration of overlap is around 0.1×10^{-2} g cm^{-3}, the threshold concentration of entanglement must be around 0.2×10^{-2} g cm^{-3} (ca. 2 times larger[31,35,38]).

For 1 M NaSal solutions of C_{16}TASal, the decrease of reciprocal scattering intensity and mutual diffusion coefficient with an increase in micelle concentration indicates the increase in micellar size. This induces the variation of virial coefficients. Therefore, the analytical procedure of light scattering for small micelles at each micelle concentration was presented.[21] That procedure was applied to 1 M NaSal solutions of C_{16}TASal.

Table II shows the numerical values evaluated by using the value of 6.55[39] for the constant, k_{f0}, in the equation

$$k_f = k_{f0}N_A[(4/3)\pi R_H^3]/M \quad (15)$$

In Table II, b is the long axis, when a prolate ellipsoid is assumed as the micelle shape instead of sphere and 2.2 nm is taken as a value of the short axis.

The size of micelles increases obviously with an increase in micelle concentration, but it depends slightly on temperature in a different way depending on micelle concentration. The second and third virial coefficients are $(0.7–2.3) \times 10^{-4}$ mol cm^3 g^{-2} and $(0.1–1.4) \times 10^{-3}$ mol cm^6 g^{-3}, respectively, and the frictional virial coefficient and the hydrodynamic virial coefficient ranges are 5–17 cm^3 g^{-1} and 0.3–1.1 cm^3 g^{-1}, respectively. The numerical values of these coefficients are consistent with those for small micelles of C_nE_7.[21]

The spinnability was observed even for aqueous solutions of C_{16}TASal without salt,[18] in which micelles take a short rod shape but the intermicellar correlation is very strong. When the micelle concentration is diluted, micelles are short and few, and the intermicellar correlation is rather weak. Then the loose pseudonetwork composed of short rodlike micelles must be formed in micellar solutions. Such a loose pseudonetwork structure can induce the spinnability with type D behavior where the drawing length is proportional to the drawing velocity.[18] The type D spinnability was observed for solutions where the viscous flow overcomes the elastic deformation.

As the micelle concentration increases, micelles lengthen, and the amount of micelles and the intermicellar correlation increase. Therefore, the pseudonetwork would tighten and such structure induces the type C spinnability, where the drawing length decreases with the drawing velocity or is independent of it and where the elastic deformation is predominant.[18] As the temperature is raised, micelles shorten. Then the pseudonetwork loosens so that the spinnability converts into type D. The possible structures of

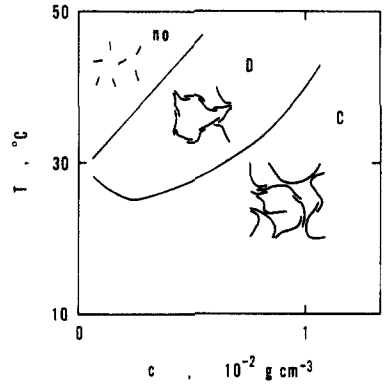

Figure 9. Possible structures of C_{16}TASal micelles in aqueous solutions without NaSal in relation to the spinnability. The diagram of spinnability was taken from ref 18. no, no spinnability; D, type D spinnability; C, type C spinnability.

C_{16}TASal micelles in aqueous solutions without NaSal are schematically drawn in Figure 9 in relation to the spinnability.

The threshold micelle concentration of entanglement may be about 2 times higher than the threshold micelle concentration of overlap,[31,35,38] which is, as a rough estimate,[37] higher than 4×10^{-2} g cm^{-3} for rodlike micelles of C_{16}TASal in aqueous solutions without NaSal. Therefore, in solutions below 10^{-2} g cm^{-3} examined in the present paper, the pseudonetwork must be constituted by the pseudolinkages but not by the entanglement. Salicylate counterions penetrated into rodlike micelles participate in the pseudolinkages, for example, by hydrogen bonding between counterions or through water, although the exact mechanism is obscure in the present situation. This kind of network is indispensable to inducing strong spinnability and viscoelasticity, because such properties are not induced from only the entanglement. Although the semidilute solutions of entangled rodlike micelles of C_{14}DAC, C_{14}DAB, and C_nE_7 exhibited strong viscosity,[40,41] they have very low viscoelasticity.

In an addition of NaSal up to 0.05–0.2 M, the intermicellar correlation diminishes but rodlike micelles lengthen. The length is 2000–3000 nm for C_{16}TASal micelles in 0.1 M NaSal. Micelles shorten at NaSal concentrations above 0.2 M, and there is no spinnability and viscoelasticity in 1 M NaSal solution where small micelles are formed. On the other hand, the constant values of the intrinsic drawing length in the type C spinnability at 25 and 35 °C had two minima at 0–0.01 M and 0.1–0.2 M NaSal.[18] The corresponding maxima in a plot of the intrinsic drawing length vs the drawing velocity at 45 °C were observed at 0–0.01 M and 0.1 M NaSal.

The complicated behavior with three extremes was also observed in plots of relaxation time vs mole ratio of NaSal to surfactant for aqueous NaSal solutions of hexadecyltrimethylammonium bromide at 25 °C[13] and in plots of zero shear viscosity and stress relaxation time as a function of surfactant concentration for aqueous NaSal solutions of hexadecylpyridinium chloride at 20 °C.[14]

In aqueous solutions of C_{16}TASal without NaSal, the pseudonetwork composed of the pseudolinkages between short rods is formed. In addition of a small amount of NaSal, the micelle growth is more dominant than the destruction of pseudolinkages by the salting-out effect. As a result, the spinnability is promoted.

(36) Ying, Q.; Chu, B. *Macromolecules* **1987**, *20*, 362.
(37) Imae, T. *Colloid Polym. Sci.* **1989**, *267*, 707.
(38) Imae, T.; Abe, A.; Ikeda, S. *J. Phys. Chem.* **1988**, *92*, 1548.
(39) Batchelor, G. K. *J. Fluid Mech.* **1972**, *52*, 245.
(40) Imae, T.; Sasaki, M.; Ikeda, S. *J. Colloid Interface Sci.* **1989**, *127*, 511.
(41) Sasaki, M.; Imae, T.; Ikeda, S. *Langmuir* **1989**, *5*, 211.

In proportion as the fraction of pseudolinkages decreases, the spinnability decreases at NaSal concentrations above the first extreme.

However, the dimension of micelle increases as NaSal is added up to the concentration of 0.05–0.2 M, and the spinnability is again promoted as the entanglement of rodlike micelles progresses. Then the pseudonetwork is constituted by the entanglement and a small fraction of pseudolinkages, and the spinnability converts from the elastic (type C) behavior at low NaSal concentrations to the viscous (type D) behavior at moderate NaSal concentrations. An addition of NaSal promotes the specific binding of salicylate counterions on a micelle. Then, since the net micelle charge decreases, the size of micelles and their entanglement increase because of the diminution of electrostatic repulsion in a micelle.

Above 0.1 M NaSal, the negative net charge of a micelle increases owing to the excess adsorption of salicylate ion. Therefore, the size of micelle diminishes, because of electrostatic repulsion in a micelle, until small micelles with negative charge are formed above 1 M NaSal. Simultaneously the spinnability decreases and disappears with the diminution and the disappearance of entanglement and pseudolinkage. Schematic models of typical micelle structures are illustrated in Figure 8.

Acknowledgment. I am grateful to Dr. Keisaku Kimura for his generous permission to use the ELS-800 instrument.

Registry No. C_{16}TASal, 61482-44-8; NaSal, 54-21-7.

Selective Reduction at the Single-Crystal Surface of All Mobile Cations in Zeolite A. Structures of Dehydrated Ag_2Ca_5–A and Ag_2Cs_{10}–A

Yang Kim,* Seong Hwan Song,

Chemistry Department, Pusan National University, Pusan 609-735, Korea

and Karl Seff*

Chemistry Department, University of Hawaii, Honolulu, Hawaii 96822-2275 *(Received: November 6, 1989; In Final Form: February 8, 1990)*

A single crystal of dehydrated Ag_2Ca_5–A (Ag^+- and Ca^{2+}-exchanged zeolite A) was treated with 0.01 Torr of Cs vapor at 200 °C for 2 h, and another such crystal was treated with 0.1 Torr of Cs vapor at 250 °C for 48 h. The product structures were determined at 21 °C by X-ray diffraction techniques in the cubic space group *Pm3m*. The composition of first crystal was Ag_2Ca_5–A (a = 12.294 (1) Å), indicating no reaction, while that of the second crystal, Ag_2Cs_{10}–A (a = 12.166 (1) Å), indicated that all Ca^{2+} ions were reduced by Cs vapor and replaced by Cs^+ ions. Full-matrix least-squares refinements of Ag_2Ca_5–A and Ag_2Cs_{10}–A converged to the final error indices, R_1 = 0.041 and R_2 = 0.048 with 227 reflections, and R_1 = 0.114 and R_2 = 0.120 with 167 reflections, respectively, for which $I > 3\sigma(I)$. In Ag_2Ca_5–A, both Ag^+ and Ca^{2+} ions lie on threefold-axis sites near 6-ring centers. In Ag_2Cs_{10}–A, both Ag^+ ions are found near 6-ring centers as before, and the 10 Cs^+ ions occupy 4 crystallographic sites: 3 Cs^+ ions lie at the centers of the 8-rings at sites of D_{4h} symmetry; 6 Cs^+ ions lie on the threefold axes of the unit cell, 4 deep in the large cavity and 2 in the sodalite cavity; one Cs^+ ion is found in the large cavity near a 4-ring. It is striking, considering the electrochemical potentials involved, to observe no reaction at all between Ag^+ and Cs^0 while simultaneously the reaction of Ca^{2+} and Cs^0 has gone to completion. It must therefore be true that Cs^0 atoms are too large to enter the 8-ring channels at 250 °C and that Ag^+ ions lack the mobility to migrate to the crystal surface for reaction. Ca^{2+} ions must have this mobility at 250 °C, as must the Cs^+ ions formed by reaction, which must therefore have occurred only at the surface of the zeolite single crystal.

Introduction

In 1956, Breck et al. reported that Cs^+ ion exchange into zeolite A with a 100% excess of Cs^+ (0.14 M aqueous solution at 90 °C) resulted in the replacement of only 31% the Na^+ ions in the zeolite A structure.[1] Barrer et al. increased the level of Cs^+ exchange to 45% by exposing the zeolite to successive concentrated aqueous solutions at 25 °C.[2] Subsequently, during the past decade, the levels of Cs^+ exchange into zeolite A were gradually increased from 7/12 to 11/12 by various ion-exchange strategies.[3-5] In 1987, Seff and Heo succeeded in preparing fully dehydrated, fully Cs^+-exchanged zeolite A by the reduction of all Na^+ ions in Na_{12}–A with cesium vapor. Complete reaction of the Na^+, K^+, Ca^{2+}, and Co^{2+} ions in dehydrated zeolite A with Cs vapor is readily achieved at 250 °C or higher.[6-8] However, when dehydrated Ag_{12}–A (an ill-defined material) was exposed to ca. 0.1 Torr of Cs vapor at 220 °C, the resulting crystal showed no single-crystal diffraction pattern, indicating that the crystallinity of the zeolite A structure had been lost.[9]

Ag^+ ions in zeolite A can be reduced by heating, by reaction with reducing agents, or by sorption of metal atoms.[10,11] In the structure of dehydrated Ag_6Na_6–A, treated with 50 Torr of H_2 at room temperature, 1.27 $(Ag_3)^+$ clusters and 0.7 $(Ag_3)^{2+}$ clusters per unit cell were found in the large cavity.[10] In the structure of $Ag_{4.6}Na_{7.4}$–A, vacuum dehydrated and treated with H_2 at 350 °C, $(Ag_6)^{3+}$ clusters of low symmetry were found in the large cavity.[11]

Barrer and Whiteman reported that large quantities of mercury vapor could be sorbed by Ag^+-exchanged zeolite X without damaging the zeolite structure.[12] However, the uptake of mercury vapor by single crystals of Ag^+-exchanged zeolite A at both 70

(1) Breck, D. W.; Eversole, W. G.; Milton, R. M.; Reed, T. B.; Thomas, T. L. *J. Am. Chem. Soc.* **1956**, *78*, 5963-5971.
(2) Barrer, R. M.; Rees, L. V. C.; Ward, D. J. *Proc. R. Soc. London, A* **1963**, *273A*, 180-197.
(3) Vance, Jr., T. B.; Seff, K. *J. Phys. Chem.* **1975**, *79*, 2163-2167.
(4) Kim, Y.; Seff, K. *Bull. Korean Chem. Soc.* **1984**, *5*, 117-121.
(5) Dejsupa, C. M. S. Thesis, University of Hawaii, 1986.
(6) Heo, N. H.; Seff, K. *J. Am. Chem. Soc.* **1987**, *109*, 7986-7992.
(7) Heo, N. H.; Dejsupa, C.; Seff, K. *J. Phys. Chem.* **1987**, *91*, 3943-3944.
(8) Heo, N. H.; Seff, K. *ACS Symp. Ser.* **1988**, *368*, 177-193.
(9) Heo, N. H. Ph.D. Thesis, University of Hawaii, 1987.
(10) Kim, Y.; Seff, K. *Bull. Korean Chem. Soc.* **1984**, *5*, 135-140.
(11) Kim, Y.; Seff, K. *J. Phys. Chem.* **1987**, *91*, 668-671.
(12) Barrer, R. M.; Whiteman, J. L. *J. Chem. Soc.* **1967**, *1967A*, 19-25.

0022-3654/90/2094-5959$02.50/0